LOWLAND TECHNOLOGY INTERNATIONAL Vol. 11, No. 2, 47-52, December 2009
International Association of Lowland Technology (IALT), ISSN 1344-9656

SOIL-WATER COUPLED ANALYSIS OF LOW LAND WIDESPREAD SUBSIDENCE DUE TO DEWATERING

K. Kaneda[1] and H. Yamazaki[2]

ABSTRACT: A series of numerical simulations of land subsidence due to dewatering were performed based on the soil-water coupled finite deformation analysis using the SYS Cam-Clay model under plane-strain conditions. The simulations showed that after land subsidence, the ground may be fragile in the event of additional loading due to disturbance of the soil structure. Ground settlement occurs with cyclic variation in ground water level, assumed to be seasonal, due to a history of water level change from extraction. Such behavior is the result of soil disturbance that occurs due to decay of the soil structure, resulting in the softening of soils through plastic volume compression.

Keywords: Numerical simulation, land subsidence, disturbance, cyclic load

INTRODUCTION

Many major cities in Asia such as Shanghai, Bangkok, Tokyo, Osaka, Nagoya and Saga have experienced widespread subsidence due to excessive extraction of water from aquifers. Fig. 1 shows the relationship between settlement of soils and time as observed on several Japanese plains. It shows that after 1960, the settlement accelerated as the Japanese economy grew. Ground water was pumped up from deep aquifers, and widespread ground subsidence occurred. In general, a clay layer from tens to hundreds of meters was sedimented onto the plain.

The mechanism of such land subsidence is decay of the soil structure (Kaneda and Matsuo, 2005). The focus of this paper is soil disturbance after dewatering. Two main topics are discussed: ongoing settlement under cyclic water level variation and numerical simulation of settlement occurring after land subsidence due to additional loading. Naturally sedimented soils are usually in a structured, overconsolidated and anisotropic state. The Super-Subloading Yield Cam-clay model with rotational hardening (SYS Cam-clay model) is powerful for incorporating these features. The behavior of softening with plastic volume compression below the critical state line, observed in highly structured clay or very loose sand, and hardening with plastic volume expansion, observed in heavily overconsolidated clay or dense sand, can be expressed using this model.

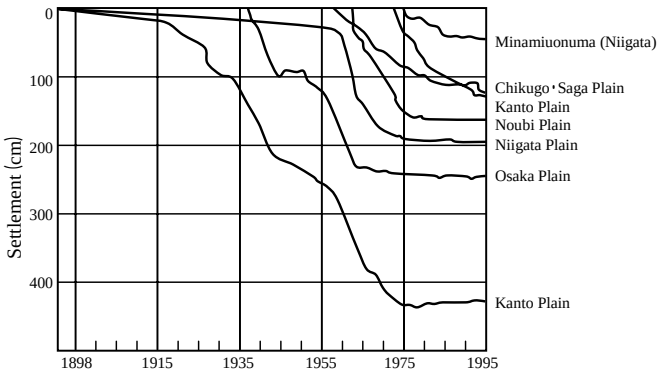

Fig. 1 Relationship between settlement and time on several Japanese plains (Ministry of the Environment, 1990)

BRIEF FORMULATION OF SYS CAM CLAY MODEL

It is assumed that the modified Cam-clay model describes the elasto-plastic response of fully destructured, normally consolidated soils. In order to explain an anisotropy or rotation of the plastic potential, the stress ratio, η^*, proposed by Sekiguchi and Ohta (1977) and Hashiguchi and Chen (1998) is introduced. In order to describe the behavior of structured soils, the concept of the superloading surface was introduced by Asaoka et. al. (2000, 2002). The superloading surface is assumed to exist in the impossible state for the modified Cam-clay, i.e., outside the Roscoe surface. The superloading surface is similar in shape to the modified Cam-clay plastic potential with its origin in the "*q-p'* space" same

[1] Takenaka Corporation, Takenaka Research & Development Institute, 1-5-1,Ohtsuka, Inzai, Chiba, JAPAN (formerly Port and airport Research Institute)
[2] Port and airport Research Institute, 3-1-1, Nagase, Yokosuka, Kanagawa, JAPAN
Note: Discussion on this paper is open until June 2010

as that of the Modified Cam-clay. The similarity ratio of the modified Cam-clay plastic potential to the superloading surface in terms of stresses, denoted by R^*, lies between zero and one. The subloading surface was introduced by Hashiguchi (1978) in order to describe the elasto-plastic behavior of overconsolidation. The natural soils are in a structured and overconsolidated state. Therefore, the current stress state of a natural soil is always on the subloading surface. The subloading surface is assumed to be geometrically similar to the superloading surface. The similarity ratio of the subloading surface to the superloading surface in terms of stresses, denoted by R, also lies between zero and one. The reciprocal of R corresponds to the overconsolidation ratio. Three surfaces and definitions of R^* and R are shown in Fig. 2. Equation (1) describes the underlying concept of the SYS model.

$$f(p',\eta^*)+\int_0^t J\mathrm{tr}\boldsymbol{D}^p d\tau+\mathrm{MDln}R^*-\mathrm{MDln}R=\mathrm{MDln}\frac{p'}{\tilde{p}_0'}+\mathrm{MDln}\frac{\mathrm{M}^2+\eta^{*2}}{\mathrm{M}^2}+\mathrm{MD}\left(\ln R^*-\ln R\right)+\int_0^t J\mathrm{tr}\boldsymbol{D}^p d\tau \tag{1}$$

where

$$\mathrm{D}=\frac{\tilde{\lambda}-\tilde{\kappa}}{\mathrm{M}(1+e)},\ J=\det\boldsymbol{F}=\frac{1+\mathrm{e}}{1+\mathrm{e}_0},\ \eta^*=\sqrt{\frac{3}{2}\hat{\boldsymbol{\eta}}\cdot\hat{\boldsymbol{\eta}}},$$
$$\hat{\boldsymbol{\eta}}=\boldsymbol{\eta}-\boldsymbol{\beta},\boldsymbol{\eta}=\frac{\boldsymbol{S}}{p'},\quad \boldsymbol{S}=\boldsymbol{T}'+p'\boldsymbol{I}\ \text{and}\ p'=-\frac{1}{3}\mathrm{tr}\boldsymbol{T}' \tag{2}$$

in which $\tilde{\lambda}$ and $\tilde{\kappa}$ are the compression and swelling indices respectively and M is the critical state parameter. $\boldsymbol{D}^p$ denotes the plastic components of the stretching tensor $\boldsymbol{D}$. Both $\boldsymbol{D}$ and $\boldsymbol{D}^p$ are defined as positive in tension. $\boldsymbol{F}$ is a deformation gradient tensor, and (1+e) and ($1+\mathrm{e}_0$) are the specific volumes at the current time $t = t$, and in the reference state $t = 0$ respectively. p' and $\boldsymbol{I}$ are the mean effective stress and unit tensor respectively, $\boldsymbol{T}'$ denotes the Cauchy effective stress tensor, and $\boldsymbol{\beta}$ is the axis of rotation tensor. The evolution law of R, R^* and $\boldsymbol{\beta}$ are as follows:

$$\dot{R}=JU\left\|\boldsymbol{D}^p\right\|,\ \dot{R}^*=JU^*\left\|\boldsymbol{D}^p\right\|\ \text{and}\ \overset{\circ}{\boldsymbol{\beta}}=J\frac{b_r}{\mathrm{D}}\sqrt{\frac{2}{3}}\left\|\boldsymbol{D}_s^p\right\|\left\|\hat{\boldsymbol{\eta}}\right\|\boldsymbol{\eta}_b \tag{3}$$

where $U=-\frac{m}{\mathrm{D}}\ln R$, $U=\frac{a}{\mathrm{D}}R^{*b}\left(1-R^*\right)^c$ and

$$\boldsymbol{D}_s^p=\boldsymbol{D}^p-\frac{1}{3}\mathrm{tr}\boldsymbol{D}^p\boldsymbol{I},\ \boldsymbol{\eta}_b=m_b\frac{\hat{\boldsymbol{\eta}}}{\left\|\hat{\boldsymbol{\eta}}\right\|}-\boldsymbol{\beta}, \tag{4}$$

$$\overset{\circ}{\boldsymbol{T}}'=\dot{\boldsymbol{T}}'+\boldsymbol{T}'\boldsymbol{\Omega}-\boldsymbol{\Omega}\boldsymbol{T}' \tag{5}$$

$$\overset{\circ}{\boldsymbol{\beta}}=\dot{\boldsymbol{\beta}}+\boldsymbol{\beta}\boldsymbol{\Omega}-\boldsymbol{\Omega}\boldsymbol{\beta} \tag{6}$$

where $\boldsymbol{\Omega}=\dot{\boldsymbol{R}}\boldsymbol{R}^T$, $\boldsymbol{R}$ is the rotation tensor and m, a, b, c, b_r and m_b are material constants. By applying the consistency condition, associated flow rule and evolution law to Equation (1), the plastic multiplier λ is obtained:

$$\lambda=\frac{\frac{\partial f}{\partial\boldsymbol{T}'}\cdot\overset{\circ}{\boldsymbol{T}}'}{J\frac{\mathrm{MD}}{p'\left(\mathrm{M}^2+\eta^{*2}\right)}\left(\mathrm{M}_s^2-\eta^2\right)} \tag{7}$$

in which

$$\mathrm{M}_s^2=\mathrm{M}_a^2+b_r\frac{4\mathrm{M}\eta^{*2}}{\mathrm{M}^2+\eta^{*2}}\left(m_b\eta^*-\sqrt{\frac{3}{2}}\hat{\boldsymbol{\eta}}\cdot\boldsymbol{\beta}\right)-\mathrm{MD}\left(\frac{U^*}{R^*}-\frac{U}{R}\right)\sqrt{6\eta^{*2}+\frac{1}{3}\left(\mathrm{M}_a^2-\eta^2\right)^2} \tag{8}$$

$$\mathrm{M}_a^2=\mathrm{M}^2+\varsigma^2 \tag{9}$$

$$\varsigma=\sqrt{\frac{3}{2}\boldsymbol{\beta}\cdot\boldsymbol{\beta}}=\sqrt{\frac{3}{2}}\left\|\boldsymbol{\beta}\right\| \tag{10}$$

The new parameter M_s is a function of the degree of structure, overconsolidation and anisotropy. Ongoing plastic deformation, value of M_s is changing up and down.

Based on the theory of plasticity, when soils are under loading, the plastic multiplier is greater than or equal to zero:

$$\lambda\geq 0 \tag{11}$$

Equation (7) shows that, for a positive λ, there are three cases of loading:

$$\begin{cases}\frac{\partial f}{\partial\boldsymbol{T}'}\cdot\overset{\circ}{\boldsymbol{T}}'>0 & \text{when}\quad \eta^2<\mathrm{M}_s^2 \quad:\quad \text{hardening}\\ \frac{\partial f}{\partial\boldsymbol{T}'}\cdot\overset{\circ}{\boldsymbol{T}}'<0 & \text{when}\quad \eta^2>\mathrm{M}_s^2 \quad:\quad \text{softening}\\ \frac{\partial f}{\partial\boldsymbol{T}'}\cdot\overset{\circ}{\boldsymbol{T}}'=0 & \text{when}\quad \eta^2=\mathrm{M}_s^2 \quad:\quad \text{perfectly plastic}\end{cases} \tag{12}$$

Since η is positive by definition, then $\eta=\mathrm{M}_s$ is found to give the threshold stress ratio between hardening and softening. Substituting an elastic response:

$$\overset{\circ}{\boldsymbol{T}}'=\boldsymbol{E}\boldsymbol{D}^e \tag{13}$$

into Equation (7), and solving with respect to λ, one gets the plastic multiplier in terms of stretching, Λ:

$$\Lambda=\lambda=\frac{\frac{\partial f}{\partial\boldsymbol{T}'}\cdot\boldsymbol{E}\boldsymbol{D}}{\frac{\partial f}{\partial\boldsymbol{T}'}\cdot\boldsymbol{E}\frac{\partial f}{\partial\boldsymbol{T}'}+J\frac{\mathrm{MD}}{p'\left(\mathrm{M}^2+\eta^{*2}\right)}\left(\mathrm{M}_s^2-\eta^2\right)} \tag{14}$$

In Equation (13), $\boldsymbol{D}^e$ denotes the elastic component of stretching, and $\boldsymbol{E}$ is the elastic modulus tensor. Employing the plastic multiplier in terms of stretching, Λ, the linear rate-type constitutive equation is obtained through:

$$\overset{\circ}{\boldsymbol{T}}' = \boldsymbol{E}\boldsymbol{D} - \Lambda \boldsymbol{E}\frac{\partial f}{\partial \boldsymbol{T}'} \tag{15}$$

When soil parameters cause the denominator to be positive, the loading criterion

$$\Lambda \geq 0 \tag{16}$$

can be rewritten simply in terms of the numerator of λ as follows:

$$\frac{\partial f}{\partial \boldsymbol{T}'} \geq 0 \tag{17}$$

Since the plastic potential surface rotates with ongoing plastic deformation, the watershed between plastic volume compression and plastic volume expansion also moves with ongoing plastic deformation. Now:

$$-\mathrm{tr}\boldsymbol{D}^p = -\lambda \mathrm{tr}\frac{\partial f}{\partial \boldsymbol{T}'} = \lambda \frac{\mathrm{MD}}{p'\left(\mathrm{M}^2 + \eta^{*2}\right)}\left(\mathrm{M}_a^2 - \eta^2\right) \tag{18}$$

The watershed between plastic volume compression and plastic volume expansion in terms of the stress ratio is given by $\eta^2 = \mathrm{M}_a^2$, which classifies volume change behavior as follows:

$$\begin{cases} -\mathrm{tr}\boldsymbol{D}^p > 0 & \text{when} \quad \eta^2 < \mathrm{M}_a^2 \quad : \quad \text{compression} \\ -\mathrm{tr}\boldsymbol{D}^p < 0 & \text{when} \quad \eta^2 > \mathrm{M}_a^2 \quad : \quad \text{expansion} \\ -\mathrm{tr}\boldsymbol{D}^p = 0 & \text{when} \quad \eta^2 = \mathrm{M}_a^2 \quad : \quad \text{no volume change} \end{cases} \tag{19}$$

The existence of the limit surface for rotational hardening gives the following constraint to M_a:

$$\mathrm{M}_a^2 \leq \mathrm{M}^2 + \frac{3}{2}m_b^2 \tag{20}$$

For further details, the reader is referred to Asaoka et. al. (2000, 2002).

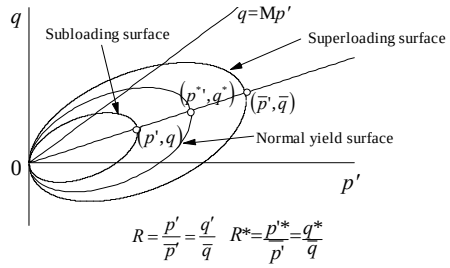

Fig. 2 Three yield surfaces

BOUNDAY CONDITIONS AND INITIAL CONDITIONS

In this paper, numerical simulations are discussed for two cases with different boundary conditions. Fig. 3(a), (b) show the boundary conditions for the two cases for a plane-strain condition: one without a sand layer at the top, and the other with a sand layer.

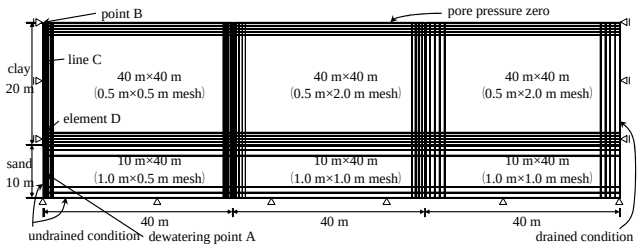

(a)

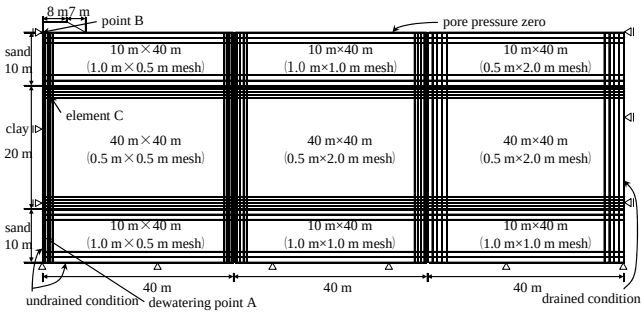

(b)

Fig. 3 Boundary conditions used in the numerical simulation in this study (a) with a sand layer on top, (b) without a sand layer on top

Table 1 Elasto-plastic parameters, evolution parameters and initial conditions

[Epasto-plastic parameters]		
	Clay	Sand
Compression index λ	0.5	0.04
Swelling index κ	0.04	0.02
Critical state constants M	1.4	1.1
Void ratio at p'=98 kPa N	2.1	2.0
Poisson's ratio ν	0.3	0.3
[Evolution parameters]		
Degradation parameter of structure a	1.0	3.0
Degradation parameter of structure b,c	1.0	1.0
Degradation parameter of overconsolidated state m	4.0	0.04
Evolution parameter of β b_r	0.001	3.0
Limit of rotation m_b	1.0	0.7
Permeability k (cm/sec)	1.0×10^{-8}	1.0×10^{-2}
Soil density ρ_s (g/cm^3)	2.60	2.65
[Initial conditions]		
State of structure $1/R^*_0$	10.0 (1.0)	1.0
O.C.R. $1/R_0$	1.6 (3.0)	10.0
Initial slope of axis of rotation ζ_0	0.23	0.23
Initial coefficient of earth pressure at rest K_0	0.5 [0.6]	0.5

The clay layer and sand layer at the bottom are the same in both cases. The top of ground was set to zero excess pore pressure, while the bottom was set as impermeable. The extraction of water was assumed to result in changes in ground water level in this study. The changing ground water level is indicated by point A in Fig. 3. The elasto-plastic parameters, evolution parameters and initial conditions used in the simulations in this study are given in Table 1. This numerical simulation was based on the soil-water coupled finite deformation analysis.

The initial distribution of water pressure is hydrostatic and initial void ratio and mean effective stress were calculated using the initial load application and self weight of both sand and clay.

NUMERICAL SIMULATIONS OF WIDESPREAD LAND SUBSIDENCE

The boundary condition modelled in the first simulation was set to Fig. 3(a) with 20 m thick clay layers and 10 m thick sand layers. The soil is in a structured, lightly overconsolidated and anisotropic state. Fig. 4 shows the initial state and distribution of p_c' for the numerical simulation. The relationships between settlement at point B in Fig. 3(a) (left axis, black line), the water level at point A (right axis, red line) and time are given in Fig. 5. In the first ten years, the water level declined to -15 m, remaining constant for the following 20 years and then recovering to -2 m after introduction of pumping control. Over one metre of settlement was observed, and after the ground water level recovered to almost its original level, rebound was almost imperceptible. Fig. 6 shows the time history of the pore pressure isochrones at line C in Fig. 3(a).Softening points coincided with delayed consolidation. The mechanism delaying consolidation with decay of structure is explained as follows: when the stress level of some soil elements reaches the domain of softening for plastic volume compression (see Equations 12 and 19), softening of a saturated soil generally yields the generation of pore pressure, which delays consolidation. Generation of pore pressure in some soil element causes unloading of nearby soil elements. After sufficient decay of structure, the stress state should lead to hardening. Therefore, the localized generation of pore pressure does not continue for long (see Kaneda and Matsuo (2005) for further details). Fig. 7 shows the shear behavior of element D on Fig. 3(a) during dewatering and recovery. Large compression occurred and plastic compression was accompanied by decay of structure ($R^*\rightarrow 1$) in v-p' space. In η, M_s-ε_s space, η exists below M_s for some time as indicated, and this is the softening time from Equation 12. Fig. 8 shows the time history of the surface geometry under dewatering and recovery. The point of dewatering is point A in Fig. 3(a), and horizontal settlement spread over 100 m. This is evidence that ground subsidence is an environmental hazard.

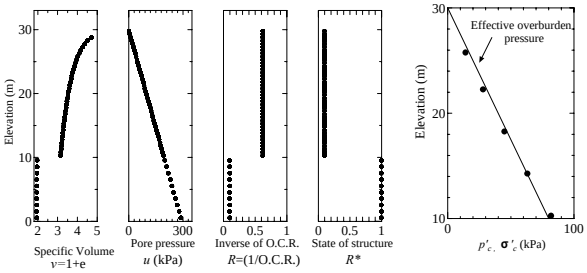

Fig. 4 Initial states used in the numerical simulation

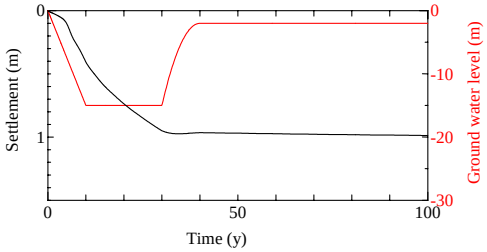

Fig. 5 Settlement at point B and ground water level at point A over time, in the numerical simulation

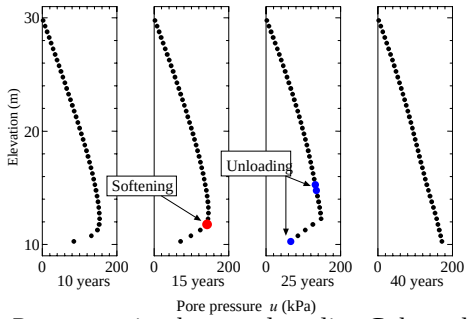

Fig. 6 Pore water isochrones along line C through time

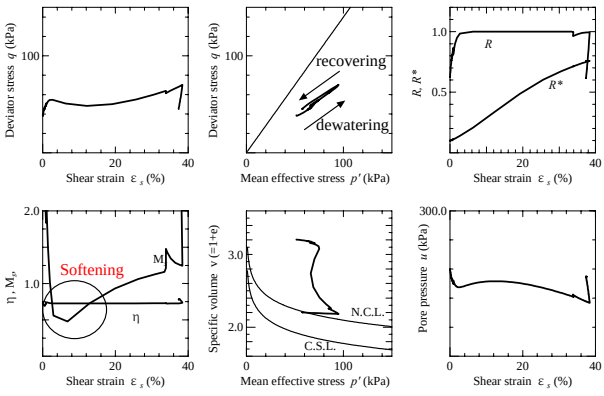

Fig. 7 Soil element behavior at element D in the numerical simulation

In general, variation in ground water level occurs seasonally. Fig. 9 shows observed groundwater levels and elevations from the Saga area (Miura et. al. 1986). In Fig. 9(a), the relationship between the variation of ground water level and elevation is irreversible, whereas

in Fig. 9(b), the relationship is reversible. For the second simulation, the material constants are given in Table 1, but the initial condition for case (a) is assumed to be a highly structured state ($1/R^*$=10, $1/R$=1.6), and case (b) is assumed to be a de-structured and lightly overconsolidated state ($1/R^*$=1.0, $1/R$=3.0). In case (a), the water level declined to -15 m over the first ten years, and then a cyclic (sine curve) water level with amplitude of 4.0 m and time period of one year was applied for 100 years. In case (b), the water level declined to -20m over the first ten years, then remained constant for the following ten years.

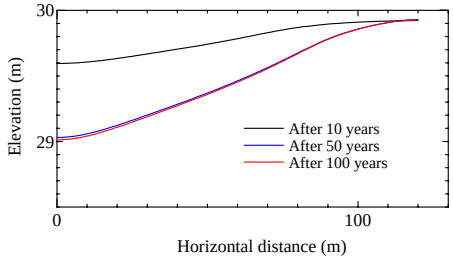

Fig. 8 Time history of ground level with horizontal distance from point A (numerical simulation)

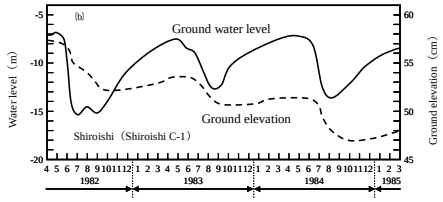

(a) Irreversible case

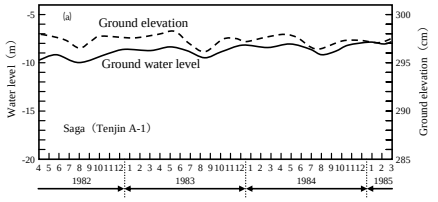

(b) Reversible case

Fig. 9 Observed ground elevation and ground water level in the Saga area

Then the water level recovered to -23 m for ten years, then a sine cyclic water level with an amplitude of 1.0 m and time period of one year was applied for 100 years. The relationships between settlement at point B and ground water level at point A for both cases are shown in Fig. 10. As for the observed data, the structured case (a) shows an irreversible relation between ground water level and settlement, whilst the de-structured, lightly overconsolidated case (b) is reversible. In case (a), softening with plastic volume compression accompanied with soil disturbance will occur under cyclic loading, because of the highly structured state. In case (b), since the overconsolidation ratio increases as the ground water level cycle is repeated, the behavior of settlement becomes elastic.

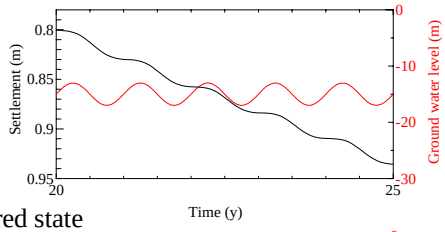

(a) Structured state

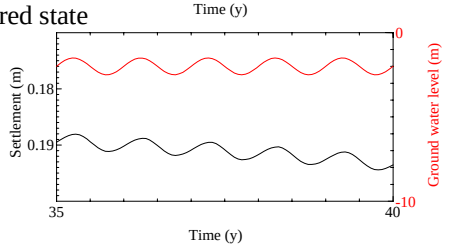

(b) De-structured, lightly overconsolidated state

Fig. 10 The results of the numerical simulation of seasonal variation in ground water level

CONTINUING FRAGILITY OF SOIL AFTER SETTLEMENT

Common-sense reasoning regarding the historical influence of past settlement might be: “Since soil settlement is consolidation caused by lowering of the ground water level, once the level is restored the result ought to be equivalent to the loading and unloading of a weight. The ground is put into an overconsolidated state, which is effectively the same as a pre-loading effect, and must result in an improvement of the soil.” In this section, we are now going to see why this argument fails to apply to a naturally deposited clay soil with a high degree of structure (Kaneda and Matsuo, 2005). The ground structure for the model simulation is set to Fig. 3(b) where there is a 10 m sand layer at the bottom, 20 m clay layer on top of the sand layer and another 10 m sand layer on top of the clay layer. The dewatering point, point A, is shown in Fig. 3(b). The material constants are shown in Table 1, but in this case, K_0 for clay was set to 0.6. For the first ten years, the water level declined to -22 m, then remained constant for the following 20 years and then recovered to its original level. At 100 years, an embankment 2.5m high is exerted on the soil surface as shown in Fig. 3(b). In the calculation, the load of the embankment is a node force and made to act on the ground surface. The unit weight of the embankment is 17 kN/m^3 and the rate of loading is 0.1 m/day. The simulated results of these changes are shown in Fig. 11. For comparison, Fig. 11 also shows a curve for a similarly loaded soil that has not undergone a history of water depletion. In the pristine soil, settlement is about 0.29 m, whilst in the soil with the depletion history, delayed settlement persists over 300 years, ending at a

level approximately 1.6 m lower than the recovery level after the previous phase of settlement. Fig. 12 shows the distribution of shear strain. The shear strain was developed firstly from the deep clay layer during dewatering, and secondly from upper clay layer after construction of the embankment. Fig. 13 shows the in-situ one-dimensional compressive response of element C in Fig. 3(b), calculated for soils with and without the history of water depletion. It is clear from this figure how a history of change in the ground water level, preserved in the form of soil disturbance, leads to a reduced reserve of so-called "preconsolidation stress p'_c". When a load is added over p'_c, delayed compression will occur. This is because settlement of soils with historical changes in water level is larger than in soils with no historical water changes. In contrast, a soil that has no depletion history of this kind will not undergo softening when subjected to a surface load.

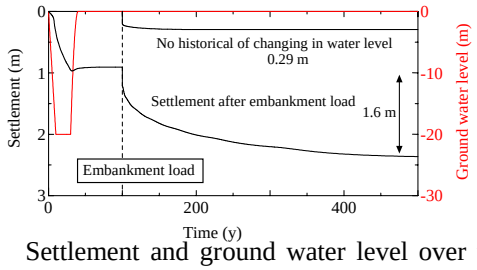

Fig. 11 Settlement and ground water level over time for a pristine soil and a disturbed soil

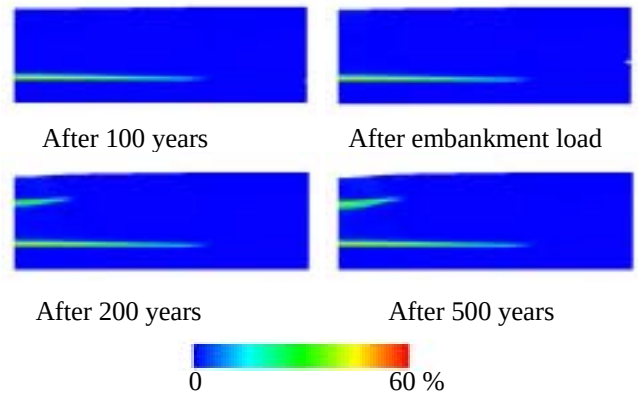

Fig. 12 Distribution of shear strain

CONCLUSION

Numerical simulations of ground subsidence on an alluvial plain were carried out using soil-water coupled analysis. The super/subloading yield surface concept and rotational hardening were employed using the modified Cam-Clay model. The plane strain analyses led to the following findings:

(1) Land subsidence caused by delayed consolidation can be observed due to the decay of soil structure in the lateral direction.

(2) Cyclic ground water variation may increase the possibility of settlement due to decay of the soil structure, caused by soil disturbance.

(3) Once exposed to subsidence of this kind, soils may remain vulnerable to further settlement under fresh loading in the future.

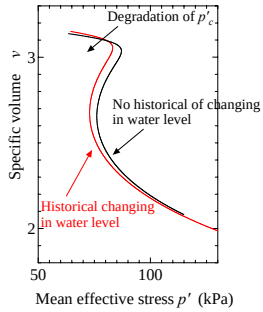

Fig. 13 Degradation of p'_c at element C

ACKNOWLEDGEMENTS

The authors wish to thank the Nagoya University soil mechanics group for helpful advice on the simulation.

REFERENCES

Asaoka, A., Nakano, M. and Noda, T. (2000). Superloading yield surface concept for highly structured soil behavior, *Soils & Foundations*, 40(2), 99-110.

Asaoka, A., Noda, T., Yamada, E., Kaneda, K. and Nakano, M. (2002). An elasto-plastic description of two distinct volume change mechanisms of soils, *Soils & Foundations*, 42(5), 47-57.

Hashiguchi, K. and Chen, Z. -P. (1998). Elastoplastic constitutive equations of soils with the subloading surface and the rotational hardening, *Int. J. Numer. Anal. Meth. Geomech*., Vol.22, 197-227.

Hashiguchi, K. (1978). Plastic constitutive equations of granular materials, *Proc. US-Japan Seminar on Continuum Mech. Stast. Appr. Mech. Granular Materials (Cowin, S.C. and Satake, M. eds.)*, Sendai, 321-329.

Kaneda, K. and Matsuo, M. (2005). Numerical simulations of low land subsidence due to dewatering using soil water coupled analysis, *16th International Conference on Soil Mechanics and Geotechnical Engineering*, Osaka, CD-ROM.

Miura, N., Isagai, K., Sakai, A. and Tohno, I. (1986). Land subsidence and quality of groundwater in Saga plain, *The Japanese Geotechnical Society, Tuchi to Kiso*, 34(11), 13-18 (in Japanese).

Ministry of the Environment, Japan (at present) (1990). *Ground subsidence and its provision*, Hakua-shobo.

Sekiguchi, H. and Ohta, H. (1977). Induced anisotropy and time dependency in clays, *Constitutive Equations of Soils* (*Proc, 9th Int. Conf. Soil Mech. Found. Eng., Spec. Session 9*), Tokyo, 229-238.